

Acceleration and dissipation statistics of numerically simulated isotropic turbulence

P. K. Yeung^{a)}

School of Aerospace Engineering, Georgia Institute of Technology, Atlanta, Georgia 30332

S. B. Pope and A. G. Lamorgese

Sibley School of Mechanical and Aerospace Engineering, Cornell University, Ithaca, New York 14853

D. A. Donzis

School of Aerospace Engineering, Georgia Institute of Technology, Atlanta, Georgia 30332

(Received 8 November 2005; accepted 31 March 2006; published online 8 June 2006)

Direct numerical simulation (DNS) data at grid resolution up to 2048^3 in isotropic turbulence are used to investigate the statistics of acceleration in a Eulerian frame. A major emphasis is on the use of conditional averaging to relate the intermittency of acceleration to fluctuations of dissipation, enstrophy, and pseudodissipation representing local relative motion in the flow. Pseudodissipation (the second invariant of the velocity gradient tensor) has the same intermittency exponent as dissipation and is closest to log-normal. Conditional acceleration variances increase with each conditioning variable, consistent with the scenario of rapid changes in velocity for fluid particles moving in local regions of large velocity gradient, but in a manner departing from Kolmogorov's refined similarity theory. Acceleration conditioned on the pseudodissipation is closest to Gaussian, and well represented by a novel "cubic Gaussian" distribution. Overall the simulation data suggest that, with the aid of appropriate parameterizations, Lagrangian stochastic modeling with pseudodissipation as the conditioning variable is likely to produce superior results. Reduced intermittency of conditional acceleration also makes the present results less sensitive to resolution concerns in DNS. © 2006 American Institute of Physics. [DOI: 10.1063/1.2204053]

I. INTRODUCTION

Because of its dual roles as the force per unit mass expressed by the Navier-Stokes equations and as the rate of change of fluid particle velocity, acceleration is a fundamental quantity in the study of turbulence in both Eulerian and Lagrangian frames of reference. Indeed in recent years the statistics of acceleration have received considerable attention.¹⁻¹³ Results from both numerical simulation (e.g., Ref. 3) and experiment (e.g., Ref. 4) have shown that the acceleration is highly intermittent, to a greater degree than observed in Eulerian velocity gradients and certainly not anticipated by classical Kolmogorov scaling. Statistical theories have been developed (Hill⁶) which interpret acceleration intermittency in terms of non-Gaussianity in the velocity field and the properties of pressure gradient fluctuations. However, the current understanding is still incomplete in key aspects such as the Reynolds-number dependence of acceleration variance in Kolmogorov variables (see, e.g., Sawford *et al.*¹¹). A satisfactory and quantitative description of the intermittency characteristics of acceleration is essential for second-order stochastic modeling based on acceleration in a Lagrangian frame (Sawford,¹⁴ Pope,⁷ Reynolds¹⁰). Clearly, for this purpose access to detailed and reliable data over a wide range of Reynolds numbers is highly desirable.

The definition of fluid particle velocity as the velocity of the fluid at the instantaneous particle position implies that

large acceleration is a natural consequence of fluid particles moving in a local region of large velocity gradients. As a result, it is useful to study the statistical relationships between acceleration and velocity gradients, which from a tensorial point of view can be decomposed into symmetric and antisymmetric parts, i.e., the strain rate $s_{ij} \equiv \frac{1}{2}(\partial u_i / \partial x_j + \partial u_j / \partial x_i)$ and rotation rate $r_{ij} \equiv \frac{1}{2}(\partial u_i / \partial x_j - \partial u_j / \partial x_i)$, where $\mathbf{u}(\mathbf{x}, t)$ denotes the Eulerian velocity field. The intensity of local straining is best measured by the second invariant of the strain-rate tensor, which upon multiplication by the viscosity ν gives the instantaneous energy dissipation rate

$$\epsilon = 2\nu s_{ij}s_{ij}, \quad (1)$$

which is in turn a key parameter in turbulence scaling (e.g., Sreenivasan¹⁵). Similarly, the second invariant of the rotation rate tensor can be used to define

$$\zeta = 2\nu r_{ij}r_{ij} = \nu \omega_i \omega_i, \quad (2)$$

which for convenience is referred to as the enstrophy (proportional to the square of vorticity ω_i), whereas the full velocity gradient tensor gives

$$\varphi = \nu \frac{\partial u_i}{\partial x_j} \frac{\partial u_i}{\partial x_j}, \quad (3)$$

which is known as the pseudodissipation. In homogeneous turbulence the quantities ϵ , ζ and φ have the same mean value but different statistics, for which Lagrangian results were first obtained by Yeung and Pope.¹⁶ Dissipation rate fluctuations are a direct measure of intermittency in turbu-

^{a)}Electronic mail: pk.yeung@ae.gatech.edu

lence and often used to represent such effects in stochastic modeling.^{17,10} However, some authors (Pope and Chen¹⁸) have found the pseudodissipation to be a more convenient alternative, especially when log-normality concepts are used in the model formulation. In addition, the pseudodissipation is often used, in the form of the second invariant of the velocity gradient tensor (mostly denoted as Q), in studies of local flow topology in turbulence (e.g., Refs. 19 and 20).

In this paper we use data from direct numerical simulations (DNS) to study the statistics of acceleration, dissipation, enstrophy, and pseudodissipation, with special interest in the statistics of acceleration conditioned upon the latter three quantities. Incidentally, relationships among acceleration, dissipation, and enstrophy were also explored recently by other authors using DNS, but at low Reynolds number.²¹ In our database the Taylor-scale Reynolds number (R_λ) ranges from about 38 on a 64^3 grid to almost 700 at resolution 2048^3 as reported recently by Yeung, Donzis, and Sreenivasan.²² A summary of the numerical approach and simulation parameters is given in Sec. II. It is well known that the Reynolds number achievable on a given grid is largely determined by the desired degree of accuracy at which the small scales are resolved. In Appendix A we address possible effects of resolution on results in this paper in view of stricter resolution requirements for DNS recently suggested in the literature (Yakhot and Sreenivasan²³). Results in the Appendix confirm that the main results in this paper (given in Secs. III and IV) are reliable, but normalized variances of acceleration and the logarithms of dissipation quantities may be underestimated by about 10%.

In Sec. III we present single-point moments of ϵ , ζ , and φ at different Reynolds numbers and compare these with predictions from log-normal theory often used in stochastic modeling. In Sec. IV we consider the variance, flatness factor, and probability density function (PDF) of acceleration fluctuations conditioned on each of the three variables ϵ , ζ or φ . Part of this work is motivated by current interest¹⁰ in stochastic modeling of acceleration using knowledge of the PDF of dissipation, and a Gaussian model for the PDF of acceleration conditional on the energy dissipation. Our results, including a highly successful fit to the acceleration PDF conditioned on pseudodissipation by a ‘‘cubic-Gaussian’’ distribution (details given in Appendix B), suggest improved model predictions are likely if conditioning on pseudodissipation is used instead. While our focus in this paper is on Eulerian aspects of the acceleration, a brief discussion of implications for Lagrangian modeling is also included in Sec. V where we summarize the conclusions of this work.

II. NUMERICAL APPROACH AND PARAMETERS

The numerical simulation and data analysis approaches used in this paper are broadly similar to those in previous work (e.g., Ref. 3), but extended to grid resolutions 1024^3 and 2048^3 using advanced Terascale supercomputer facilities currently available. Stationary homogeneous isotropic turbulence forced stochastically at the large scales (Eswaran and Pope²⁴) was simulated using the Fourier pseudospectral al-

TABLE I. Basic simulation parameters at different grid resolutions.

Grid	64^3	256^3	512^3	1024^3	2048^3
R_λ	40	139	238	385	680
L_1/η	22	101	191	449	747
$\langle \epsilon \rangle L_1/u'^3$	0.709	0.463	0.431	0.443	0.393
S_ϵ	0.537	0.521	0.549	0.580	0.622

gorithm of Rogallo²⁵ in a parallel code adapted for the efficient use of as many as 2048 parallel processors. Postprocessing codes are used to process archived instantaneous Eulerian velocity fields separated by time intervals of order half a large-eddy turnover time and treated as independent realizations for ensemble averaging. Differentiations necessary to calculate velocity gradients in the definitions of ϵ , ζ , and φ are readily performed in Fourier space. Acceleration is calculated via the Navier-Stokes equations as the sum of the pressure gradient and viscous contributions to the specific force causing the acceleration. Pressure fluctuations are recovered by solving a Poisson equation in a pseudospectral manner, with aliasing errors carefully controlled by a combination of phase-shifting and truncation techniques in wave number space.

The processing of conditional statistics is in principle straightforward but some care is needed to address the issue of limited sampling at the tails of the PDF of the conditioning variable. For the conditional PDFs of acceleration we use the notation $f_{a|X}(\hat{a}|\hat{X})$, where a is any coordinate component of the acceleration, X is any of the three invariants ϵ , ζ , and φ , and carets ($\hat{\cdot}$) denote sample-space variables. Because of intermittency, the PDFs of these conditioning variables possess wide tails, where accurate sampling is difficult because of the limited number of samples. However, because of approximate log-normal behavior it is convenient, and easier, to condition on the logarithms instead, with results presented in terms of $Y = \log_{10}(X/\langle X \rangle)$. The sampling range we use corresponds to $\{-5, 5\}$ for the standardized logarithm of X , i.e., $Z \equiv (\ln X - \langle \ln X \rangle)/\sigma_{\ln X}$, where $\sigma_{\ln X}$ denotes the standard deviation of $\ln X$. Since Z is approximately Gaussian we can use the properties of the Gaussian distribution to choose wider bins near the tails of the distribution so that better sampling within each bin leads to smoother results for the sampled PDF and conditional expectations.²⁶ It is still inevitable, though, that higher-order moments are subject to larger uncertainty due to greater sensitivity to the tails of the PDF of the conditioning variable. Confidence intervals are calculated and used²⁷ as diagnostic measures of statistical data quality.

Table I summarizes some basic parameters of the simulation database analyzed in this paper. The range of length scales present in the flow is given by the ratio between the longitudinal integral length scale (L_1) and the Kolmogorov scale (η). The normalized mean dissipation rate $\langle \epsilon \rangle L_1/u'^3$ (where u' is the standard deviation of a velocity component) is of order 0.4. This is consistent with known DNS data in both decaying and forced isotropic turbulence (see Sreenivasan²⁸), although different values are known in ex-

perimental data in other geometries.²⁹ The dissipation skewness S_ϵ (which should not be confused with the skewness of dissipation fluctuations) is (see Kerr³⁰) a measure of the shape of the energy spectrum $E(k)$ through the integral $\int k^4 E(k) dk$ which is sensitive to contributions from high wave numbers. In the case of isotropic turbulence at sufficiently high Reynolds number S_ϵ is also (Batchelor³¹) equal to the negative of the skewness of a longitudinal velocity gradient (e.g., $\partial u_1 / \partial x_1$), which in turn is known to increase slightly at higher Reynolds numbers.³² The results are subject to considerable statistical variability which is caused by both the stochastic nature of the forcing scheme and the limitations of a finite-size domain whose linear dimensions are only a few times as much as the large-eddy length scales. Since this variability extends to the Reynolds number as well, for some of our results (in Sec. III, especially) scatter plots where each realization is represented by one data point provide more information than plots of ensemble averages at an averaged Reynolds number for each simulation. Some basic aspects such as evidence of an inertial range in the energy spectrum have been reported recently in Ref. 22.

In the simulations listed in Table I the degree of resolution of the small scale motions is given by the parameter $k_{\max} \eta$ at about 1.5 where $k_{\max} = \sqrt{2N/3}$ is the highest resolvable wave number (allowing for dealiasing treatments) on an N^3 grid of length 2π in each direction. Correspondingly the ratio of grid spacing (Δx) to the Kolmogorov length scale (η) is given by $(2\pi\sqrt{2/3}) / (k_{\max} \eta) \approx 2$. Although this means motions at scale sizes smaller than η are not well resolved this is also common practice in the field for simulations aimed at reaching the highest Reynolds number possible for a given amount of computational resources available. In Appendix A we compare results from three simulations at nominally the same Reynolds number but different values of $k_{\max} \eta$ that correspond to $\Delta x / \eta \approx 2, 1,$ and $1/4$. The errors involved are found to be relatively small.

III. MOMENTS OF DISSIPATION QUANTITIES AND ACCELERATION

The variance of the logarithm of dissipation is a basic measure of intermittency which is known to increase with Reynolds number. According to the Refined Similarity Hypotheses (RSH) proposed by Kolmogorov³³ this dependence can be expressed as

$$\sigma_{\ln \epsilon}^2 = A + (3\mu/2) \ln R_\lambda, \quad (4)$$

where A depends on large-scale motions of length L , η is the Kolmogorov scale, μ is called an intermittency exponent, and the scale estimate $L/\eta \sim R_\lambda^{3/2}$ has been used. Figure 1 shows results for the variance of the logarithms of ϵ , ζ , and φ , with data from each simulation at a different grid resolution represented by a separate cluster of points. Corresponding ensemble averages which are useful for model comparisons are given in Table II. It is clear that all three quantities display a logarithmic dependence on the Reynolds number, with a faster rate of increase for the enstrophy but about the same between energy dissipation and pseudodissipation. Equation (4) and its analogs for ζ and φ correspond to

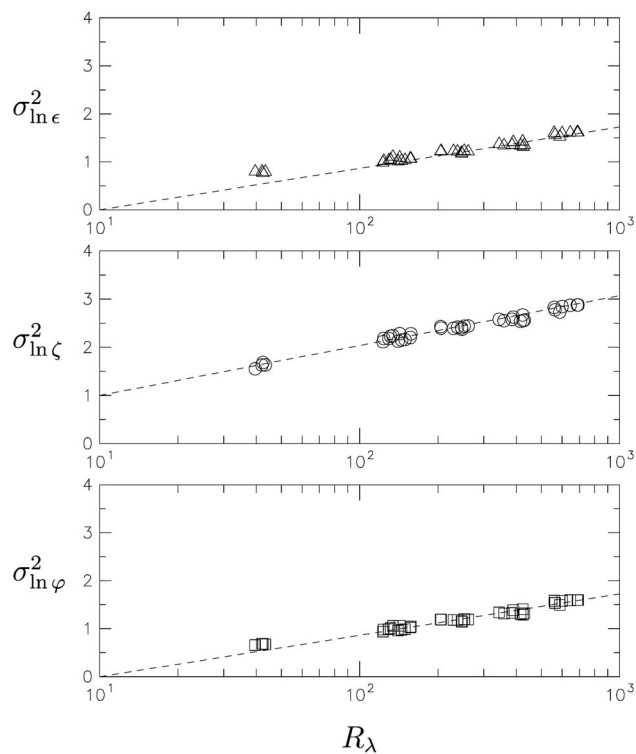


FIG. 1. Reynolds number scaling of the variances of (from top) $\ln \epsilon$ (Δ), $\ln \zeta$ (\circ) and $\ln \varphi$ (\square) obtained from DNS at grid resolutions from 64^3 to 2048^3 (see Table I). Each data point represents one realization of an instantaneous velocity field in statistically stationary state. Dashed lines represent [see Eq. (4)] $A = -0.863$, $\mu = 0.25$ for $\ln \epsilon$ and $\ln \varphi$; $A = 0.036$, $\mu = 0.3$ for $\ln \zeta$.

dashed lines of slope $(3\mu/2) \ln 10$ shown in the figure. Excellent agreement is seen with $\mu = 0.25$ for the dissipation as reported in experiments,³⁴ and with a larger value $\mu = 0.3$ for enstrophy.

Obukhov³⁵ introduced the concept of log-normal distributions for intermittent, non-negative variables that represent the small scales in turbulence. Despite having some known physical limitations³⁶ log-normal assumptions are often useful in stochastic modeling. A basic test of log-normality is presented here in Figs. 2 and 3 via data on the skewness (μ_3) and flatness (μ_4) factors of the logarithms, in the same scatter-plot format as in Fig. 1. Both of these figures suggest that (as in Yeung and Pope¹⁶) φ is in general closest to log-normal, followed by ϵ . Log-normality for ζ is also seen to be a better approximation at high Reynolds numbers although a definitive statement on the asymptotic $R_\lambda \rightarrow \infty$ limit cannot be made on the basis of the data available.

For a further check on log-normality we show in Fig. 4 PDFs of the logarithms of ϵ , ζ , and φ , using ensemble-averaged results at the highest Reynolds number in our 2048^3 simulation. These PDFs display departures from symmetry which are consistent, in both magnitude and sign, with the skewness factors in Fig. 2. For example, for enstrophy (which is the most intermittent of these three variables), the log-normal model underestimates the likelihood of very low values corresponding to large, negative $\ln \zeta$ while overestimating the far tails of the PDF representing the most intense fluctuations of ζ . Comparison of Fig. 4 with similar plots at

TABLE II. Ensemble-averaged moments at different grid resolutions. Numbers in the bottom two rows marked by the † are from Lagrangian data.

Grid	64 ³	256 ³	512 ³	1024 ³	2048 ³
R_λ	40	139	238	385	680
$\sigma_{\ln \epsilon}^2$	0.815	1.071	1.237	1.390	1.616
$\sigma_{\ln \zeta}^2$	1.653	2.224	2.440	2.610	2.858
$\sigma_{\ln \varphi}^2$	0.704	1.032	1.209	1.364	1.596
a_0	1.27	2.74	3.40	3.97	4.54
$\mu_4(a)$	7	20	40	68	107
† a_0	1.34	2.68	3.37	3.84	4.42
† $\mu_4(a)$	7	19	36	47	60

lower Reynolds numbers (not shown) is also in accord with Figs. 2 and 3 in indicating that departures from log-normality become weaker at increasing Reynolds number.

Before we present the statistics of acceleration conditioned upon the velocity gradient invariants ϵ , ζ , and φ , it is appropriate to use data from the latest simulations to update some previous DNS results on (unconditional) acceleration statistics also computed in an Eulerian frame. A basic and still unresolved issue is whether the acceleration variance obeys a result obtained by direct application of Kolmogorov scaling,³⁷ i.e., whether the quantity

$$a_0 = \frac{\langle a^2 \rangle}{\langle \epsilon \rangle^{3/2} \nu^{-1/2}} \quad (5)$$

is a universal constant at sufficiently high Reynolds number. Several different results for the scaling of acceleration variance have been given in the literature.^{38,2,3,39,6,11} In particular, based on data at R_λ up to 240 from 512³ simulations, Vedula and Yeung³ suggested an $R_\lambda^{1/2}$ dependence dominated by

pressure gradient intermittency whereas the much smaller viscous part is likely to be universal. Figure 5 shows a scatter plot of all data points available from the present simulations, while corresponding ensemble averages are found in Table II. It is clear that data points from 1024³ and 2048³ simulations follow a weaker Reynolds number dependence than previously proposed. Instead, the DNS data are well represented by two formulas given by Sawford *et al.*,¹¹ namely

$$a_0 = 5/(1 + 110/R_\lambda), \quad (6)$$

which in principle implies an asymptotic limit of $a_0=5$, and

$$a_0 = 1.9R_\lambda^{0.135}/(1 + 85/R_\lambda^{1.135}), \quad (7)$$

which approaches a power law of exponent 0.135 suggested by a multifractal intermittency model by Borgas.⁴⁰ As Sawford *et al.*¹¹ noted, these two formulas (solid curve and dotted curve) are, fortuitously, almost identical up to R_λ nearly 10³, which implies that the present Reynolds numbers are still not sufficiently high to resolve the issue. We also see, in

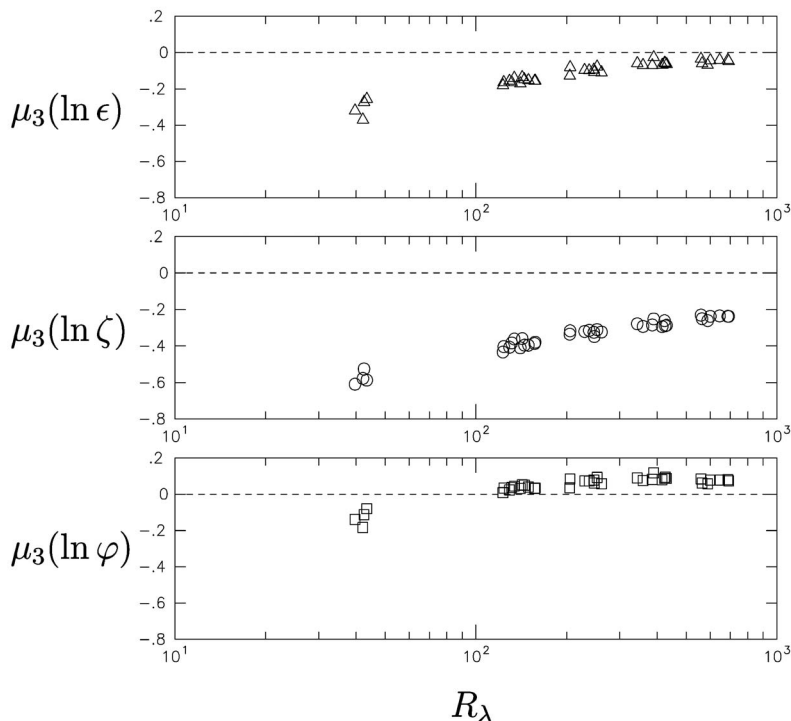


FIG. 2. Skewness factor of the logarithms of ϵ , ζ and φ corresponding to the data in Fig. 1.

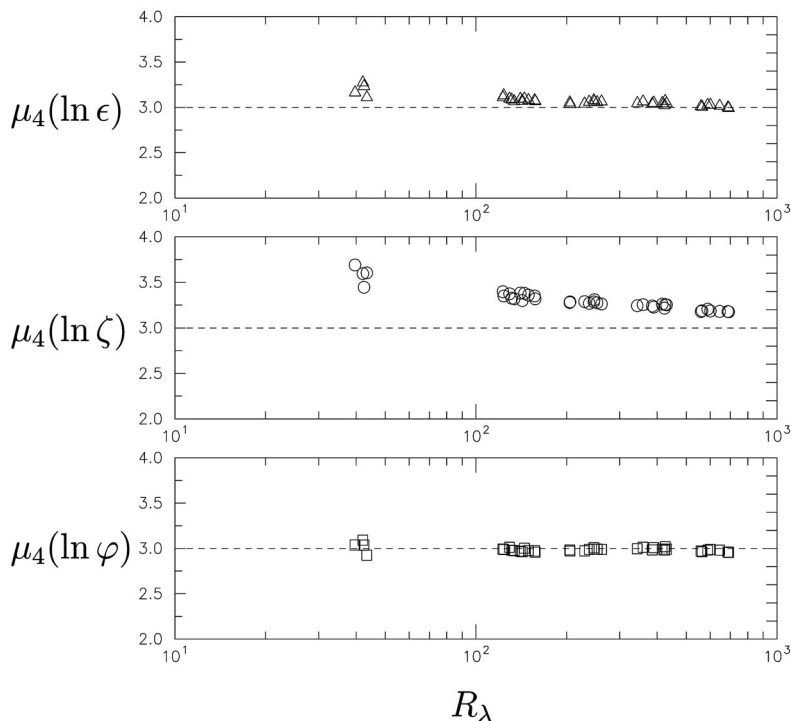


FIG. 3. Flatness factor of the logarithms of ϵ , ζ and φ corresponding to the data in Fig. 1.

the lower panel of this figure, that values for the viscous part (which is solenoidal) from the 2048³ simulation are slightly larger than suggested by other data points. This can be related to a slight increase³ at high Reynolds number for the dissipation skewness (see Table I).

The general relation for the m th order moment of a log-normal distribution (e.g., Pope⁴¹)

$$\langle X^m \rangle / \langle X \rangle^m = \exp \left[\frac{1}{2} m(m-1) \sigma_{\ln X}^2 \right] \tag{8}$$

allows us to assess to what extent the observed scaling of a_0 can be explained by an intermittency correction based on log-normal theory. Setting $m=3/2$ in Eq. (8) gives $\langle \epsilon^{3/2} \rangle / \langle \epsilon \rangle^{3/2} = \exp(\frac{3}{8} \sigma_{\ln \epsilon}^2)$, whereupon we can write

$$\tilde{a}_0 = \frac{\langle a^2 \rangle}{\langle \epsilon^{3/2} \rangle \nu^{-1/2}} = a_0 \exp \left(-\frac{3}{8} \sigma_{\ln \epsilon}^2 \right). \tag{9}$$

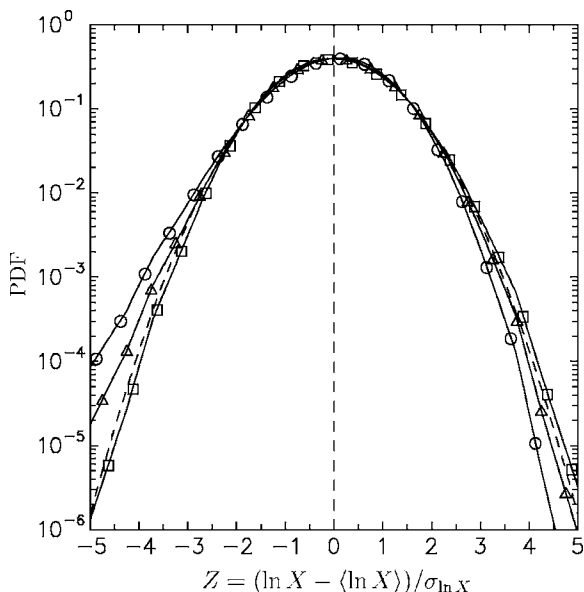


FIG. 4. Standardized PDFs of $\ln \epsilon$ (Δ), $\ln \zeta$ (\circ) and $\ln \varphi$ (\square) from 2048³ simulation at $R_\lambda \approx 680$. The dashed curve (a parabola) represents a standard Gaussian distribution for comparison.

In other words log-normal theory predicts asymptotic constancy for \tilde{a}_0 such that a_0 is proportional to $\exp(\frac{3}{8} \sigma_{\ln \epsilon}^2)$ (which increases with the Reynolds number). This is tested in Fig. 6, which shows a_0 as a function of $\sigma_{\ln \epsilon}^2$ compared to the dashed line $a_0 = 2.3 \exp(\frac{3}{8} \sigma_{\ln \epsilon}^2)$. It is far from convincing that the data are approaching an asymptote $a_0 \sim \exp(\frac{3}{8} \sigma_{\ln \epsilon}^2)$, but at the same time this behavior cannot be ruled out. In any case, substitution for $\sigma_{\ln \epsilon}^2$ from Eq. (4) leads to a predicted Reynolds number scaling $R_\lambda^{9\mu/16}$. Use of the empirical value $\mu=0.25$ gives $(9\mu/16)=0.141$, which is close to and again difficult to distinguish from the $R_\lambda^{0.135}$ asymptote based on Eq. (7) above. (It may be noted that even at $R_\lambda=1000$ the scaling factors $R_\lambda^{0.141}$ and $R_\lambda^{0.135}$ differ by only 4%, which is well within the range of numerical uncertainty.)

Almost all of the acceleration results in this paper are obtained from Eulerian processing as described at the beginning of Sec. II. However, at the bottom of Table II we also include results from Lagrangian processing, where we calculate acceleration by finite differencing of the fluid particle velocity which is in turn obtained by cubic-spline interpola-

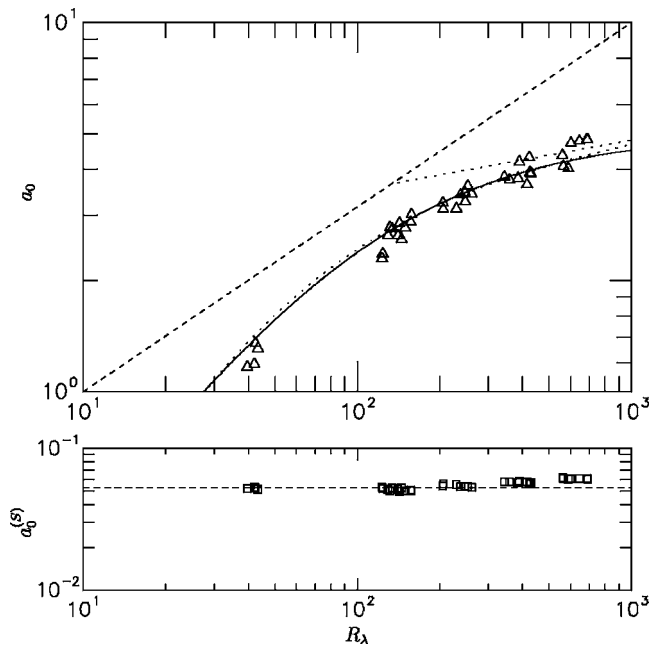


FIG. 5. Reynolds number dependence of the Kolmogorov-scaled acceleration variance (a_0) and its solenoidal part ($a_0^{(s)}$) due to viscosity. The data are compared with: $a_0 \sim R_\lambda^{1/2}$ (dashed line), Eq. (6) (solid curve), Eq. (7) (dotted curve), and $a_0 \sim R_\lambda^{0.135}$ (dotted line). The dashed line in the bottom panel is 0.53 (see Ref. 3).

tion from Eulerian velocity fields. It is well known that in homogeneous turbulence one-particle, one-time Lagrangian statistics are in principle equivalent to single-point Eulerian statistics. However, small differences in our results can occur for several reasons, including statistical sampling, errors from interpolation, errors from time differencing of the velocity time series, and numerical forcing used in the equations of motion which determine the particle velocity. It is encouraging to note that Eulerian and Lagrangian acceleration variances in Table II agree to within just a few percent. At the same time, because the types of errors cited here lead

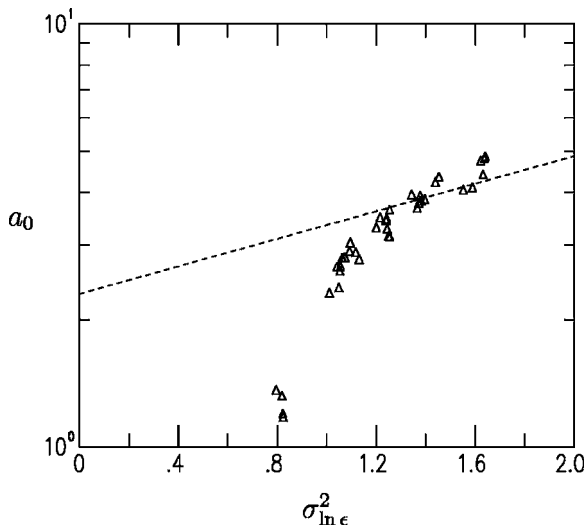


FIG. 6. Kolmogorov-scaled acceleration variance versus variance of the logarithm of dissipation. The dashed line is $a_0 = 2.3 \exp(\frac{2}{8} \sigma_{\ln \epsilon}^2)$ [see Eq. (9)].

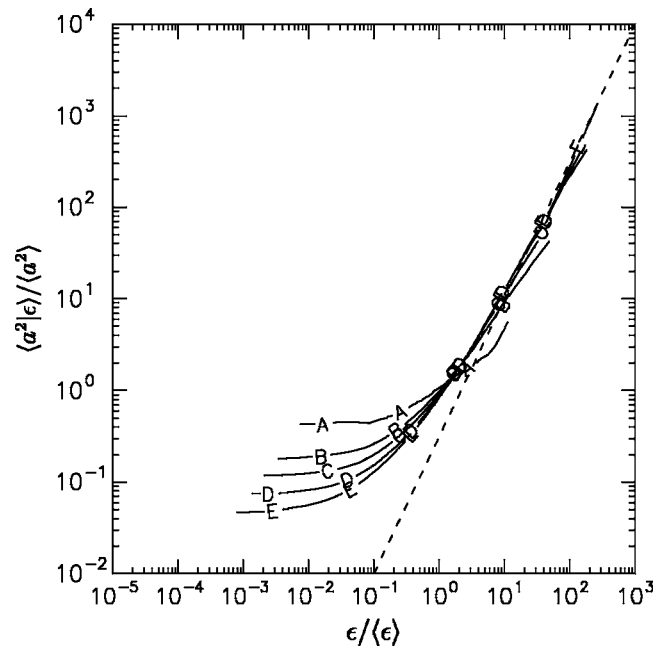


FIG. 7. Normalized conditional acceleration variance given the energy dissipation. Lines A–E are for simulations at grid resolutions 64^3 , 256^3 , 512^3 , 1024^3 , and 2048^3 with Reynolds numbers as given in Table I. A dashed line of slope 1.5 is drawn for comparison with Kolmogorov’s refined similarity theory.

to local smoothing in both time and space, it is not a surprise that the Lagrangian flatness factor is systematically smaller, especially at high Reynolds number.

IV. CONDITIONAL ACCELERATION STATISTICS

Knowledge of conditional averages is valuable because they provide a quantifiable measure of the statistical coupling between fluctuations in one flow variable and another, and because they arise as unclosed terms in stochastic modeling applied to PDF equations. For example, Sawford *et al.*¹¹ considered acceleration fluctuations given the velocity, in directions parallel and perpendicular to the fluctuating velocity vector, whereas Borgas and Yeung⁴² focused on results for use in modeling of two-particle dispersion. Here we study the acceleration given the dissipation, enstrophy, or pseudodissipation. These choices are motivated in part by a desire to provide useful information for stochastic modeling,^{18,10} and to understand in greater detail the different physical effects of strain-rate and rotation-rate fluctuations which are dominated by the small-scale motions.

Figures 7–9 show data at several Reynolds numbers (see Table I) for the conditional acceleration variance normalized by its unconditional mean, i.e., $\langle a^2 | X \rangle / \langle a^2 \rangle$ as functions of $X / \langle X \rangle$ where $X = \epsilon, \zeta, \text{ or } \varphi$. All of the curves shown are relatively smooth, which indicates satisfactory statistical sampling. As expected, the acceleration increases with all three conditioning variables, especially when the latter are large, thus demonstrating that local relative motion contributes naturally to rapid changes in fluid particle velocity. The dependence on X is relatively weak for small X , and the conditional variance at $X = \langle X \rangle$ is close to the unconditional

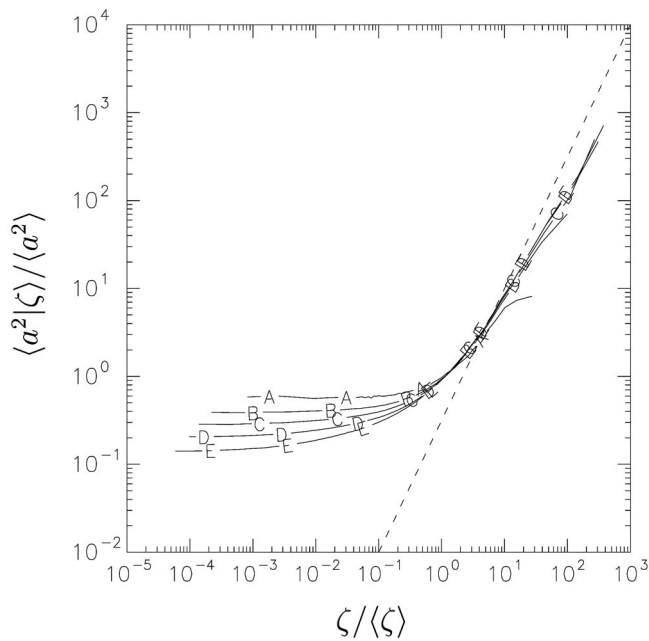


FIG. 8. Same as Fig. 7, but for conditioning on the enstrophy.

value. It is clear that the contrast between results at small and large X (where a power law may provide a reasonable fit) becomes greater at higher Reynolds numbers.

While most curves in Figs. 7–9 follow the general trends noted above, some systematic differences can also be observed. For each given conditioning variable increased intermittency at high Reynolds number is reflected in a wider spread along the $X/\langle X \rangle$ axis (due to a larger variance of $\ln X$) and a greater increase of the conditional variance at large $\langle X \rangle$ as fluctuations of greater intensity arise. Results for all three conditioning variables $X = \epsilon, \zeta$ or φ at the highest Reynolds number available are shown together for comparison in Fig. 10. A dashed line represents a power law of 1.5 predicted by the

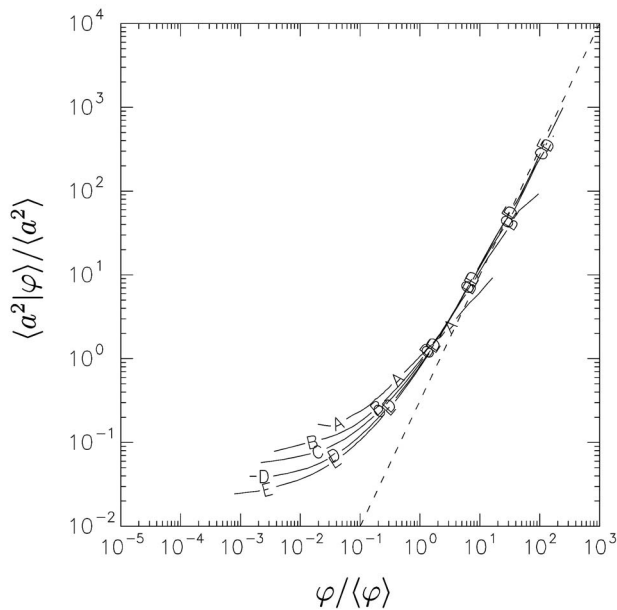


FIG. 9. Same as Fig. 7, but for conditioning on the pseudodissipation.

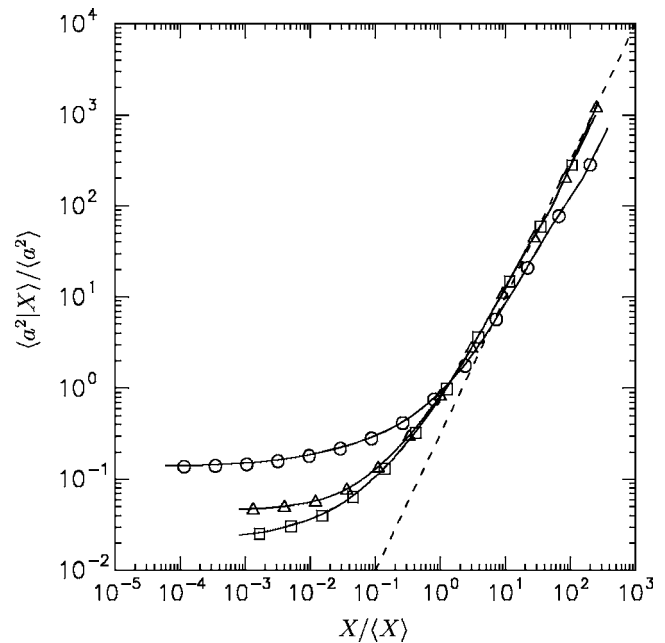


FIG. 10. Comparison of normalized conditional acceleration variances given ϵ (Δ), ζ (\circ) or φ (\square), from 2048³ simulations at $R_\lambda \approx 680$.

hypotheses of Kolmogorov³³ and Obukhov.³⁵ Although the last few data points at largest $\epsilon/\langle \epsilon \rangle$ and $\varphi/\langle \varphi \rangle$ appear to approach this slope the overall trend is consistent with a lower slope. Furthermore, conditioning on enstrophy produces a clearly less rapid increase, with a slope of roughly 1.2. In other words, “large dissipation” tends to give a larger acceleration than “large enstrophy” does. This suggests acceleration fluctuations of the highest intensity are more likely to be a result of fluid particles moving in regions of large strain rate (dissipation) than large rotation rate (enstrophy).

For modeling purposes, it is useful to obtain an accurate parameterization of the conditional variance on the pseudo-dissipation in terms of both the conditioning value and the Reynolds number. A closer examination of the results in Figs. 7–9 suggests that an empirical fit of the form $\alpha(\varphi/\langle \varphi \rangle)^{0.15} + \beta(\varphi/\langle \varphi \rangle)^{1.25}$ may be applicable, where α and β are factors depending on R_λ , specifically

$$\frac{\langle a^2 | \varphi \rangle}{\langle \epsilon \rangle^{3/2} \nu^{-1/2}} = \frac{1.2}{R_\lambda^{0.2}} \left(\frac{\varphi}{\langle \varphi \rangle} \right)^{0.15} + \ln \left(\frac{R_\lambda}{20} \right) \left(\frac{\varphi}{\langle \varphi \rangle} \right)^{1.25}, \quad (10)$$

which in Fig. 11 is shown to represent the DNS data at $R_\lambda \geq 140$ remarkably well. The closeness of the fit is illustrated by the facts that the average error is just 6%, and that the maximum error is 21% (in the last two data points of largest $\varphi/\langle \varphi \rangle$ at the highest Reynolds number), even as the conditional variance varies over four orders of magnitude.

The two terms contributing to the empirical expression above for $\langle a^2 | \varphi \rangle$ above are dominant at small and large values of $\varphi/\langle \varphi \rangle$ respectively. For large $\varphi/\langle \varphi \rangle$ as the Reynolds number increases the second term becomes more important but there is no evidence for a power-law exponent to increase from 1.25 to the value 1.5 suggested by the conventional interpretation of the refined Kolmogorov hypotheses. (Note

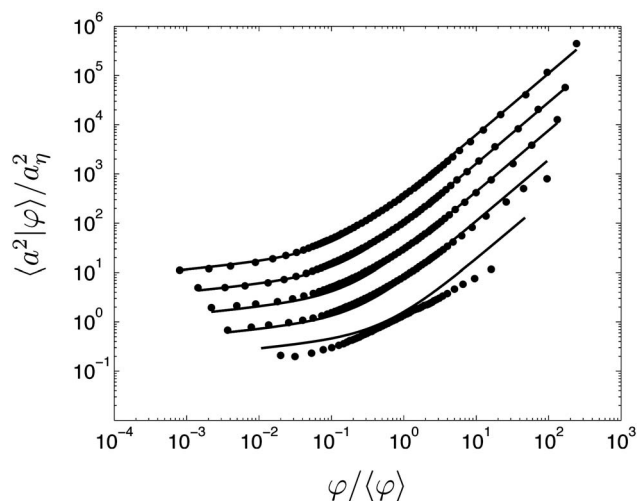


FIG. 11. Acceleration variance conditional on the pseudodissipation, φ , normalized by the Kolmogorov acceleration $a_\eta \equiv ((\epsilon)^3/\nu)^{1/4}$. [Note $a_\eta^2 \equiv (\epsilon)^{3/2}\nu^{-1/2}$.] The symbols are the DNS data; the lines are the empirical fit, Eq. (10). The lowest curve and the y axis correspond to the 64^3 simulation. The other four curves are for the 256^3 , 512^3 , 1024^3 , and 2048^3 simulations, successively shifted upwards by a factor of $\sqrt{10}$.

that, as originally formulated,^{33,35} the refined Kolmogorov hypotheses pertain only to inertial-range statistics.)

A consistency check can be applied to the empirical relation (10) for the conditional variance by requiring that, in combination with a model for the PDF of φ as the conditioning variable, it reproduces the DNS data on the unconditional variance. From the assumption of log-normality for φ and empirical data on the Reynolds number dependence of $\sigma_{\ln \varphi}^2$ [in the form of Eq. (4), with $\mu=0.25$] one obtains the following prediction for the unconditional acceleration variance,

$$\frac{\langle a^2 \rangle}{\langle \epsilon \rangle^{3/2} \nu^{-1/2}} = \frac{1.3}{R_\lambda^{0.22}} + 0.88 R_\lambda^{0.06} \ln \left(\frac{R_\lambda}{20} \right). \quad (11)$$

It may be noted that the increase in $\sigma_{\ln \varphi}^2$ with R_λ is expressed by the weak contribution $R_\lambda^{0.06}$, whereas (over the Reynolds numbers considered) the dominant term in Eq. (11) is $\ln(R_\lambda/20)$ which is derived from the empirical fit [Eq. (10)] to the conditional acceleration variance.

Recent developments in stochastic modeling associated with the so-called superstatistical approach^{9,10} have included the assumption that the acceleration is conditionally Gaussian, i.e., the conditional PDF of acceleration given the dissipation is taken to be Gaussian for all values of the dissipation (Reynolds *et al.*⁴³). The concept of a Gaussian conditional acceleration can be interpreted as implying that intermittency in acceleration is due purely to intermittency in the chosen conditioning variable. (For example if we consider two normalized random variables X and Y and represent their relationship as $Y=bX+\xi$ where b is a fixed coefficient and ξ is an uncorrelated Gaussian random noise, then the conditional PDF of Y given X equal to some prescribed X_0 is Gaussian; this implies any intermittency in Y must be due to the same in X .)

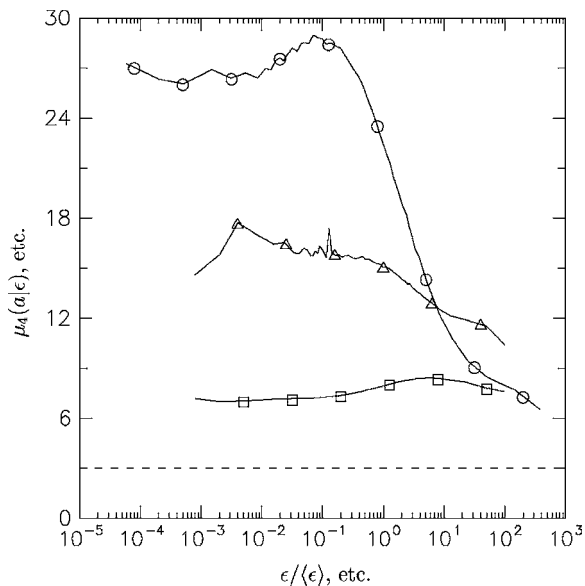


FIG. 12. Conditional flatness factor of acceleration given ϵ (Δ), ζ (\circ) or φ (\square), from 2048^3 simulation at $R_\lambda \approx 680$.

A convenient test of conditional Gaussianity is through the conditional flatness factor

$$\mu_4(a|\epsilon = \hat{\epsilon}) \equiv \frac{\langle a^4 | \epsilon = \hat{\epsilon} \rangle}{\langle a^2 | \epsilon = \hat{\epsilon} \rangle^2}, \quad (12)$$

which we also write as $\mu_4(a|\epsilon)$ for short and would be 3.0 if the conditional PDF is exactly Gaussian. Because of the denominator in its definition, the conditional flatness factor is not constrained by expressions of the type $\langle a^m \rangle = \int \langle a^m | \epsilon = \hat{\epsilon} \rangle f_\epsilon(\hat{\epsilon}) d\hat{\epsilon}$ that relate conditional and unconditional moments of order m . However, the observed behavior of $\mu_4(a|\epsilon)$ is expected to lie between two extremes: namely (i) equal to unity in the degenerate case where a is a deterministic function of ϵ (although the terminology of “flatness factor” would then be inappropriate), and (ii) equal to the (high) unconditional flatness factor if a were statistically independent of ϵ . It should also be noted that, because (according to the data in Figs. 7–10) the denominator in Eq. (12) is a strong function of the conditioning variable, acceleration fluctuations contributing to a large conditional flatness may not necessarily be very large in absolute terms.

Figure 12 shows conditional flatness based on ϵ , and on ζ and φ [defined similarly as in Eq. (12)] in the 2048^3 simulation. Clearly, the observed values are much smaller than the unconditional flatness (given in Table II), and conditioning on φ produces the closest approximation to conditional Gaussianity. Both $\mu_4(a|\epsilon)$ and $\mu_4(a|\zeta)$ are largest at relatively small values of the conditioning ϵ and ζ , respectively, whereas the dependence of $\mu_4(a|\varphi)$ on conditioning φ is relatively weak. This behavior of $\mu_4(a|\epsilon)$ and $\mu_4(a|\zeta)$ suggests that intermittent fluctuations of the acceleration can occur in either regions of low strain rate (but high rotation), or, with greater probability, regions of low rotation rate (but high strain). In other words, although both large ϵ and large ζ can independently cause large acceleration, usually these effects do not occur together.

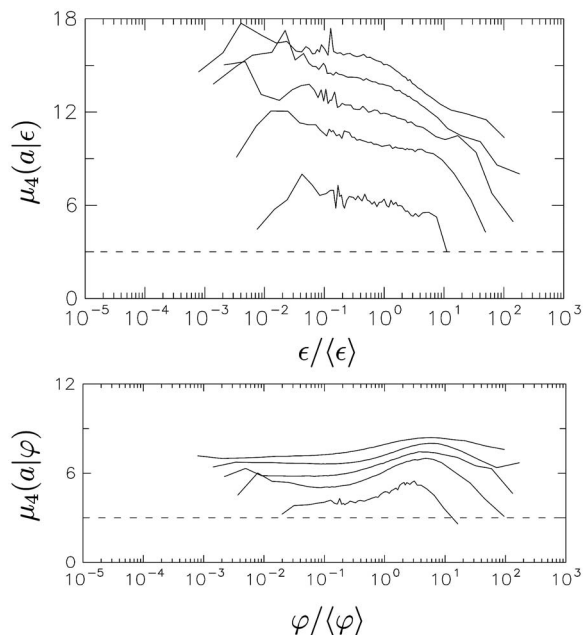


FIG. 13. Conditional flatness factor of acceleration given ϵ (top) and φ (bottom), in simulations at resolutions 64^3 to 2048^3 with Reynolds numbers as given in Table I. The data values increase monotonically with Reynolds number.

Since the pseudodissipation incorporates contributions from both strain rate and rotation rate it can be expected to capture intermittency in the acceleration more completely. This should in turn lead to a lower conditional flatness factor $\mu_4(a|\varphi)$, which is indeed observed in Fig. 12. Close observation shows that $\mu_4(a|\varphi)$ appears to take a mild maximum at moderately large values of the pseudodissipation, on the order of $10\langle\varphi\rangle$, which may again correspond to samples where an intense fluctuation occurs for either strain rate or rotation rate, but not both simultaneously. Nevertheless, the profile of $\mu_4(a|\varphi)$ can be considered approximately flat. This is convenient in practice because it allows the use of a simpler model for the conditional PDF with no dependence on the conditioning variable.

For information on the Reynolds number dependence of the conditional flatness factors we show in Figs. 13(a) and 13(b) data on $\mu_4(a|\epsilon)$ and $\mu_4(a|\varphi)$ from simulations at different grid resolutions. A general increase with the Reynolds number consistent with the unconditional flatness is observed, with greater sensitivity in the case of $\mu_4(a|\epsilon)$. This suggests that models which assume conditional Gaussianity for acceleration given the dissipation are likely to incur greater errors at high Reynolds number.

From Figs. 12, 13(a), and 13(b) it is clear that the assumption of conditionally Gaussian acceleration is more (although not totally) satisfactory if the pseudodissipation instead of dissipation is used as the conditioning variable. Further information can be obtained from the conditional PDFs, i.e., $f_{a|\epsilon}(\hat{a}|\hat{\epsilon})$ and $f_{a|\varphi}(\hat{a}|\hat{\varphi})$ which can be readily obtained as the ratio of the joint PDF (of a and $X=\epsilon, \zeta$ or φ) to the marginal PDF of each conditioning variable. In Figs. 14 and 15 and we show these conditional PDFs extracted from the 2048^3 simulation and compared with the unconditional

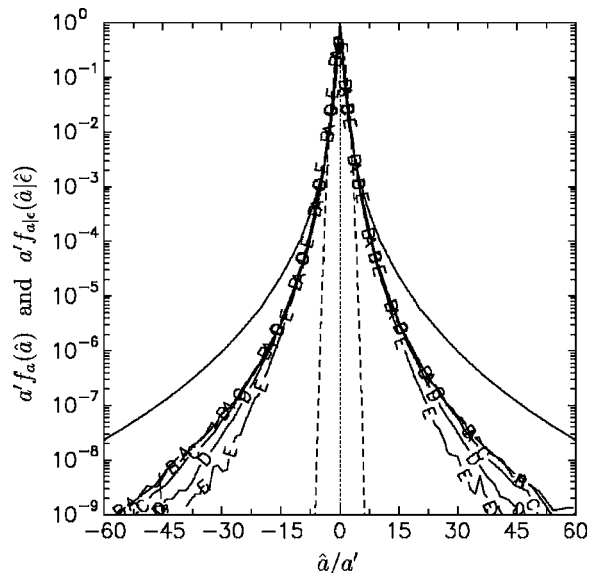


FIG. 14. Standardized conditional PDFs of acceleration given the dissipation from 2048^3 simulations at $R_\lambda \approx 680$. Lines A–E are for $\hat{\epsilon}/\langle\epsilon\rangle = \{0.0359, 0.136, 0.469, 1.62, 6.05\}$ (corresponding to $Z \equiv (\ln \hat{\epsilon} - \langle \ln \hat{\epsilon} \rangle) / \sigma_{\ln \hat{\epsilon}} = \{-2.054, -0.994, 0, 0.994, 2.054\}$). The data are compared to the unconditional PDF of acceleration (unmarked solid line) and a standard Gaussian (dashed curve). The fluctuation \hat{a} is normalized by a rms value (a') specific to each curve.

acceleration PDF (unmarked solid line). To facilitate an assessment of conditional Gaussianity we have normalized the acceleration fluctuation by its *conditional* rms for five chosen values of the conditioning variables, corresponding closely to fluctuations of $\ln \epsilon$ or $\ln \varphi$ at $-2, -1, 0, 1,$ and 2 standard deviations from their mean. It can be seen that both sets of conditional PDFs display much less intermittent behavior (with weaker tails at large fluctuations) than the unconditional PDF. This is especially true for conditioning on the pseudodissipation, which however still exhibits a significant

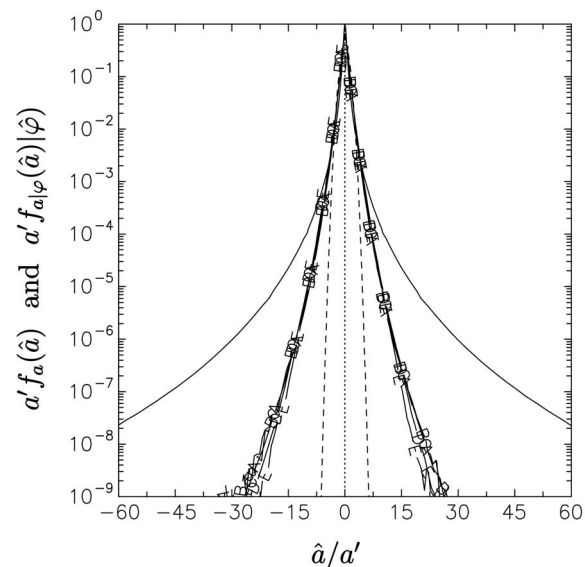


FIG. 15. Same as Fig. 14, but for conditioning on the pseudodissipation. Lines A–E are for $\hat{\varphi}/\langle\varphi\rangle = \{0.0362, 0.134, 0.458, 1.56, 5.79\}$ (corresponding to $Z \equiv (\ln \hat{\varphi} - \langle \ln \hat{\varphi} \rangle) / \sigma_{\ln \hat{\varphi}} = \{-2.054, -0.994, 0, 0.994, 2.054\}$).

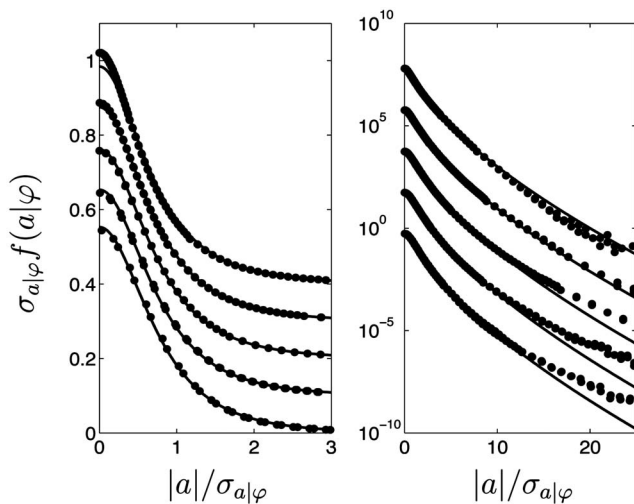


FIG. 16. Standardized conditional PDFs of acceleration, $f_{a|\varphi}(\hat{a}|\hat{\varphi})$, conditioned on pseudodissipation. The symbols are from the 2048³ DNS; the lines are the cubic Gaussian PDF with the same flatness factor as the DNS data. The values of the conditioning variable are $(\ln \varphi - \langle \ln \varphi \rangle) / \sigma_{\ln \varphi} = \{-2.054, -0.994, 0, 0.994, 2.054\}$. On each plot, the lower curve and the y axis correspond to the lowest conditioning value. The curves for the other conditioning values are successively shifted upwards, by an amount of 0.2 on the linear plot (on the left), and by a factor of 100 on the logarithmic plot (on the right).

departure from Gaussianity. A remarkable degree of collapse of these conditional PDFs for different values of the conditioning variables is also apparent except for very small and very large conditional fluctuations. The tails of the conditional PDFs for the two largest conditioning values are seen to lie “inside” those for smaller values of the conditioning variables. This is consistent with the decrease of conditional flatness factor at large ϵ or φ seen in Figs. 12, 13(a), and 13(b).

The shapes of the PDFs of acceleration conditional on pseudodissipation are further examined in Fig. 16 (on both linear and logarithmic scales). The standardized PDFs shown are from the 2048³ simulations; the five PDFs for the five values of the conditioning variable are offset vertically for clarity; and, since the PDFs are symmetric, they are plotted against $|\hat{a}|/\sigma_{a|\varphi}$ (where $\sigma_{a|\varphi}$ is the conditional standard deviation $\langle a^2|\varphi \rangle^{1/2}$). The lines shown in the figure are the *cubic Gaussian* PDFs having the same values of the flatness factor as the experimental PDFs. The definition and properties of the cubic Gaussian distribution are given in Appendix B. A cubic Gaussian random variable is simply the weighted sum of a Gaussian random variable and its cube. As may be seen, the cubic Gaussian provides a remarkably accurate representation of the conditional PDFs extracted from the simulations. The principal observable difference is that, for the lower values of the conditioning variable, the far tails of the PDFs from the DNS (beyond 12 standard deviations, say) are somewhat above the cubic Gaussian.

For simulations at lower Reynolds number the agreement between the data on $f_{a|\varphi}(\hat{a}|\hat{\varphi})$ (not shown) with the cubic Gaussian is comparable to that shown in Fig. 16. On the other hand, for $f_{a|\epsilon}$ and $f_{a|\zeta}$ although the cubic Gaussian provides a less accurate representation, it is still qualitatively

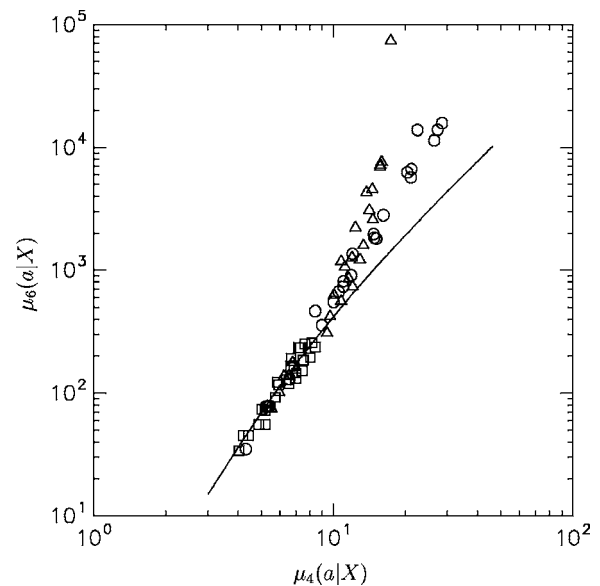


FIG. 17. Plot of conditional superskewness (μ_6) versus conditional flatness (μ_4) of acceleration, for the conditioning variable being $X = \epsilon$ (Δ), ζ (\circ), and φ (\square). DNS data from simulations at 5 grid resolutions and at 5 values of the conditioning variable as in Fig. 16 in each case are shown. Larger numerical values are generally those found at higher Reynolds numbers. The existence of one extreme data point at $\mu_6(a|\epsilon)$ nearly 10^5 is an indication of statistical uncertainty in the higher-order moments. The solid line represents the cubic-Gaussian fit to the conditional PDF.

correct and significantly more accurate than an Gaussian assumption.

To help assess the closeness of fit for higher-order conditional moments we show in Fig. 17 DNS data on the superskewness plotted against the flatness factor for the conditional acceleration PDF. Results for all three conditioning variables and all Reynolds numbers available are included. Also shown is the line corresponding to the cubic Gaussian. As may be seen, the data for conditioning on pseudodissipation have relatively low flatness factors (less than 9, as previously mentioned) and lie close to the cubic Gaussian line. In contrast, conditioning on dissipation or enstrophy generally leads to a larger flatness factor, as well as a superskewness which lies above the cubic Gaussian line.

The cubic Gaussian is a new distribution in turbulence research. While its ability to represent the data in Fig. 16 is quite striking, we offer no physical or statistical explanation for the observed agreement. In stochastic models for acceleration, the cubic Gaussian is readily achieved as the cubic of a Gaussian stochastic process. Since PDFs with approximately stretched exponential tails are ubiquitous in turbulence, a question for future research is whether there are additional statistics with the cubic Gaussian distribution.

V. CONCLUSIONS AND DISCUSSION

In this paper we have used data from direct numerical simulations of isotropic turbulence to investigate the statistics of acceleration, with a focus on conditional statistics which relate acceleration intermittency to parameters of local relative motion in the flow. The dissipation, enstrophy and pseudodissipation [Eqs. (1)–(3)] are used as conditioning

TABLE III. Comparisons of statistics of dissipation, enstrophy, pseudodissipation, and acceleration obtained from simulations of different grid resolution at nominally the same Reynolds number ($R_\lambda \approx 140$).

Grid	256 ³	512 ³	2048 ³
$k_{\max} \eta$	1.4	2.8	11.0
$\sigma_{\ln \epsilon}^2$	1.07	1.13	1.14
$\sigma_{\ln \zeta}^2$	2.22	2.32	2.36
$\sigma_{\ln \varphi}^2$	1.03	1.10	1.15
$\mu_3(\ln \epsilon)$	-0.15	-0.10	-0.12
$\mu_3(\ln \zeta)$	-0.39	-0.37	-0.36
$\mu_3(\ln \varphi)$	0.04	0.08	0.06
$\mu_4(\ln \epsilon)$	3.10	3.11	3.10
$\mu_4(\ln \zeta)$	3.36	3.37	3.34
$\mu_4(\ln \varphi)$	2.99	3.03	3.00
a_0	2.74	3.13	3.03
$\mu_4(a)$	20	27	26

variables. The grid resolution is up to 2048³ and the corresponding Taylor-scale Reynolds number is close to 700. Some of the simulation data are examined closely from a modeling point of view and compared with predictions from Kolmogorov's refined similarity theory at high Reynolds number.

Statistics of the logarithms of dissipation, enstrophy, and pseudodissipation in our DNS database are found to be consistent with a well-defined intermittency exponent which is essentially the same for dissipation and pseudodissipation ($\mu=0.25$) but larger for enstrophy ($\mu=0.3$). As in previous results at lower Reynolds number,¹⁶ the pseudodissipation is closest to having a log-normal distribution which also becomes a better approximation for enstrophy as the Reynolds number increases. The present data are also used to revisit the unresolved issue of Kolmogorov scaling of the (unconditional) acceleration variance. However, the present Reynolds numbers are still not sufficiently high to distinguish clearly between some estimates proposed in the literature based on intermittency models for energy dissipation fluctuations.

Acceleration variances conditioned on dissipation, enstrophy or pseudodissipation generally show a strong dependence at large values of these conditioning variables, which is consistent with the expectation of rapid changes of velocity for fluid particles moving in local regions of high strain, rotation, or large velocity gradients in general. However, the observed dependence departs from the prediction of the refined Kolmogorov hypotheses, especially at small values of the conditioning variable. For application in modeling we have developed two-term functional fits [Eqs. (10) and (11)] for the acceleration variance conditioned on pseudodissipation and the corresponding unconditional variance assuming a log-normal distribution for pseudodissipation fluctuations.

The assumption of conditionally Gaussian acceleration (Reynolds *et al.*⁴³) is tested by computing conditional flatness factors and probability density functions (PDF). It is found that the assumption holds best (although not perfectly) if the pseudodissipation instead of energy dissipation is chosen as the conditioning variable. Conditional flatness factors,

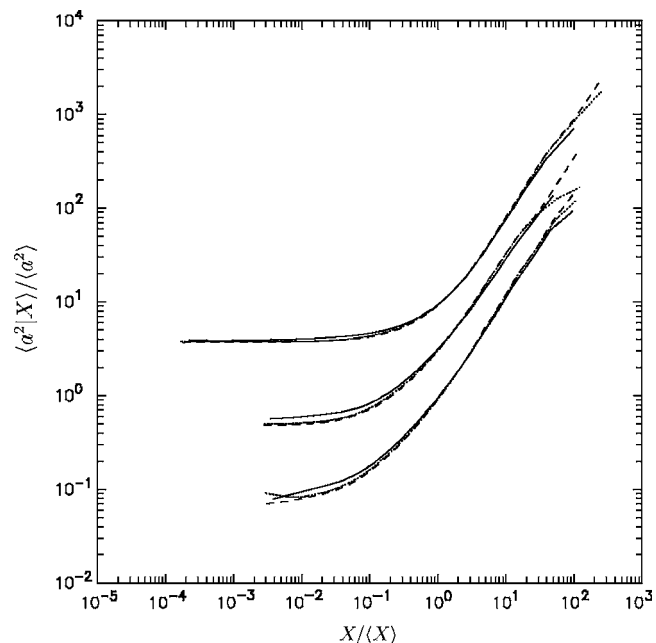


FIG. 18. Normalized conditional acceleration variances for each conditioning variable (from top to bottom) $X=\zeta$, ϵ or φ from simulations at the same Reynolds number ($R_\lambda \approx 140$) but different grid resolutions (see Table III). Solid, dashed, and dotted lines denote simulations with 256³, 512³, and 2048³ grid points, respectively (corresponding to $\Delta_x/\eta \approx 2, 1,$ and $1/4$). For clarity, curves for conditioning on enstrophy and dissipation are shifted upwards by factors of 10 and $\sqrt{10}$.

which are much lower than the unconditional values, indicate the extent to which acceleration intermittency is the result of intermittency in the chosen conditioning variable. Flatness factors conditioned on pseudodissipation up to 8 are observed (compared to the Gaussian value of 3). Our data suggest that intense acceleration may occur either in regions of high dissipation and low enstrophy or high enstrophy and low dissipation. However both of these lead to high pseudodissipation which thus captures most occurrences of large acceleration. The PDF of acceleration conditioned on φ is found to be remarkably insensitive to the value of φ , only weakly dependent on the Reynolds number, and represented remarkably well by a ‘‘cubic Gaussian.’’ As described in Appendix B, this distribution is the PDF of the weighted sum of a Gaussian random variable and its cube.

In summary, the results of this paper indicate a strong connection between the turbulence fluctuations of acceleration and pseudodissipation, which is expected to lead to a fruitful path for including the effects of intermittency and Reynolds number in stochastic modeling. The data given in this paper are almost exclusively Eulerian. Corresponding Lagrangian studies including modeling based on the present results are to be reported separately.

ACKNOWLEDGMENTS

We gratefully acknowledge support from the National Science Foundation, via Grant No. CTS-0328314 (P.K.Y.) and CTS-0328329 (S.B.P.). Large allocations of computational resources were provided by the U.S. Department of Energy (through an Office of Science INCITE Award) at the

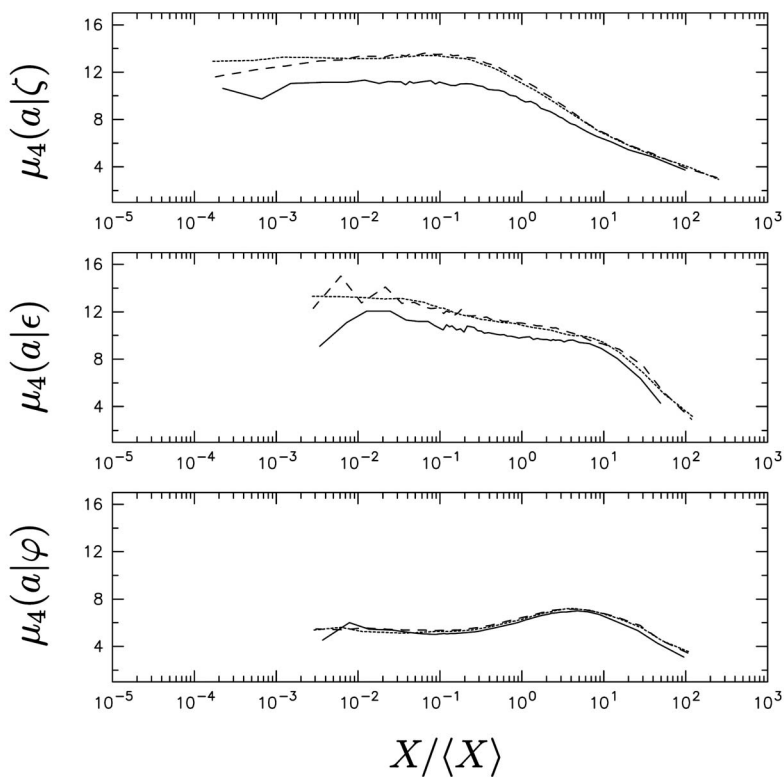


FIG. 19. Conditional flatness factors of acceleration given (from top to bottom) $X=\zeta$, ϵ or φ for the same datasets as in Fig. 18. Solid, dashed, and dotted lines denote simulations with 256^3 , 512^3 , and 2048^3 grid points respectively.

NERSC facility at Lawrence Berkeley National Laboratory, and by San Diego and Pittsburgh Supercomputer Centers which are both supported by NSF. We also thank Professor B. L. Sawford, Professor K. R. Sreenivasan, and Professor A. Tsinober for very helpful comments and suggestions.

APPENDIX A: RESOLUTION EFFECTS ON DNS RESULTS

In DNS at a given Reynolds number and grid resolution, it is known that^{44,45} uncertainty in results for higher-order moments increases with the order of the moment. This occurs for both deterministic and statistical reasons, namely, that numerical methods of finite accuracy may not be capturing the most intense intermittent fluctuations, and that higher-order moments are sensitive to the occurrence of such large fluctuations which are relatively rare and hence difficult to sample adequately. Recently, Yakhot and Sreenivasan²³ have proposed theoretical arguments based on high Reynolds number intermittency which suggest more stringent resolution requirements than levels commonly practiced in DNS. Here we do not attempt rigorous testing of the new theory, but instead limit ourselves to checking resolution effects by comparing results at different grid resolutions for a moderate Reynolds number ($R_\lambda \approx 140$). As stated in Sec. II the resolutions employed correspond to $\Delta/\eta \approx 2$, 1, and $1/4$; the actual values of $k_{\max}\eta$ are, as given in Table III, 1.4, 2.8, and 11, but for convenience we refer to them below as (nominally) ≈ 1.5 , 3, and 12.

Table III shows comparisons for quantities corresponding to those in Table II, and Figs. 2 and 3. As measures of intermittency the computed values of logarithmic variances

of ϵ , ζ , and φ are expected to increase with a degree of resolution. These increases are seen to be of order 10% between $k_{\max}\eta \approx 1.5$ and 12, with most of the difference being between results at $k_{\max}\eta \approx 1.5$ and 3. Skewness and flatness factors of the logarithms show very little change, which suggests resolution has little effect on conclusions regarding log-normal behavior (or deviation therefrom). The acceleration variance increases by about 10%–15%, whereas the acceleration flatness factor (which is a more sensitive indicator of intermittency) increases more strongly, by about 30%. Both the variance and flatness factor are slightly less at $k_{\max}\eta \approx 12$ than at $k_{\max}\eta \approx 3$, which suggests that results at these two resolution levels are within statistical margins of each other.

Figure 18 shows comparisons for conditional variances (corresponding to data in Figs. 7–9). To help separate each group of curves from one another we have shifted data for conditioning on enstrophy and dissipation by constant factors as stated in the figure captions. It is clear that the resolution effects are relatively small, and that results at $k_{\max}\eta \approx 3$ and 12 differ very little except for some sampling noise at extremely large values of each conditioning variable. Very similar features are also found at the fourth-moment level, for conditional flatness factors which are shown in Fig. 19. Agreement between results at different resolution levels is particularly striking for acceleration conditioned on the pseudodissipation, which is the least intermittent compared with conditioning on dissipation or enstrophy. Clearly, this result is also a favorable indicator of the robustness of modeling based on pseudodissipation as the conditioning variable.

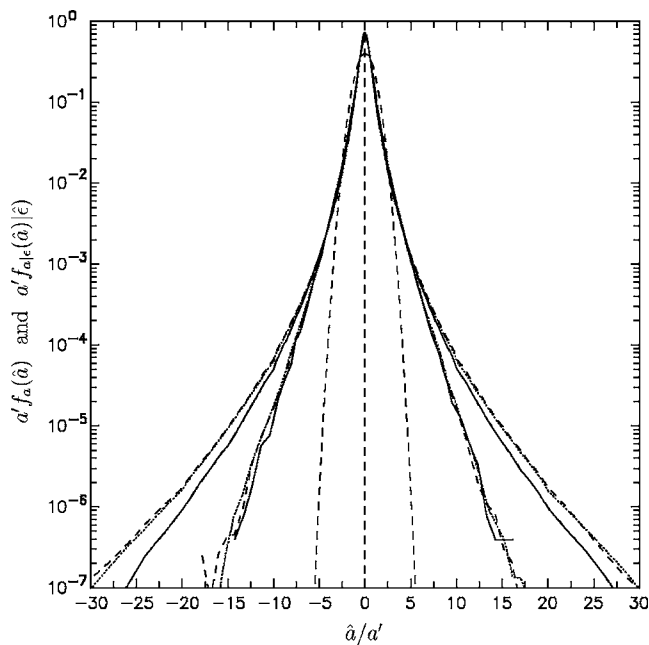


FIG. 20. Unconditional PDF of acceleration (outer lines) and corresponding conditional PDFs (inner lines) given relatively high dissipation $[\ln \epsilon - \langle \ln \epsilon \rangle] / \sigma_{\ln \epsilon} \approx 2$ for the same datasets as in Fig. 18. Solid, dashed, and dotted lines denote simulations with 256^3 , 512^3 , and 2048^3 grid points respectively. As in Figs. 14 and 15 the fluctuation \hat{a} is normalized by a rms value (a') specific to each curve, and a dashed parabola for the standard Gaussian is shown for comparison.

Conditional flatness factors in Fig. 19 are much less sensitive to resolution effects than unconditional flatness factors in Table III. Correspondingly, one can expect that conditional PDFs are also less sensitive to resolution than the unconditional PDF. This contrast is confirmed in Fig. 20, which also shows that unconditional PDFs for $k_{\max} \eta \approx 3$ and 12 are almost identical up to about 30 standard deviations from the mean (although significant differences may still arise in the extreme tails of the PDF representing yet-larger fluctuations).

The fact that differences between $k_{\max} \eta \approx 3$ and 12 are very small and most likely within statistical error confirms that $k_{\max} \eta \approx 3$ can be considered “accurate,” and that comparison between $k_{\max} \eta \approx 1.5$ and 3 is a fair measure of error in the former. Overall, the results in this Appendix suggest strongly that, despite recent concerns about effects of intermittency on resolution requirements in DNS, the main conclusions of this paper remain valid. It is, of course, quite possible that these effects will become stronger at high Reynolds number, where high-resolution data needed for rigorous testing are not yet available. However, it is also clear that the reduced intermittency of conditional variables leads to much more robust results, especially for modeling based on the pseudodissipation.

APPENDIX B: PROPERTIES OF THE CUBIC GAUSSIAN DISTRIBUTION

In Sec. IV the cubic Gaussian distribution as defined below has been found to provide an excellent representation for the PDF of acceleration conditioned on the pseudodissi-

pation. Below we provide the definition of this distribution and a brief account of its basic properties.

Let X be a standardized Gaussian random variable. Then, for a given value of the parameter p ($0 \leq p \leq 1$), the random variable

$$Z \equiv C[(1-p)X + pX^3], \quad (\text{B1})$$

is called a standardized cubic Gaussian [denoted as $G^3(p)$], where the constant C (dependent on p)

$$C = (1 + 4p + 10p^2)^{-1/2}, \quad (\text{B2})$$

is determined by the standardization condition $\langle Z^2 \rangle = 1$. Thus Z is the weighted sum of a Gaussian X and its cube X^3 , where the weighting factors $C(1-p)$ and Cp are decreasing and increasing functions of p , respectively.

Let $G(x)$ and $g(x) \equiv \frac{1}{\sqrt{2\pi}} e^{-x^2/2}$ denote the cumulative distribution function (CDF) and the probability density function (PDF) of the standardized Gaussian. Then the CDF of the cubic Gaussian is

$$F_p(z) \equiv \text{Prob}\{Z < z\} = G(\hat{x}(z, p)), \quad (\text{B3})$$

where $\hat{x}(z, p)$ denotes the unique solution to

$$z = C[(1-p)\hat{x} + p\hat{x}^3]. \quad (\text{B4})$$

The PDF of Z , $f_p(z)$, is given by

$$f_p(z) = g(\hat{x}) d\hat{x}/dz = \frac{\exp\left(-\frac{1}{2}\hat{x}^2\right)}{\sqrt{2\pi}C(1-p+3p\hat{x}^2)}. \quad (\text{B5})$$

Properties of the $G^3(p)$ distribution include the following:

(1) The PDF $f_p(z) = f_p(-z)$ is symmetric and standardized [$\langle Z \rangle = 0$, $\text{var}(Z) = 1$].

(2) All moments $\mu_n(p) \equiv \langle Z^n \rangle$ exist and are simply related to those of the Gaussian. In particular the flatness factor is

$$\mu_4(p) = 3(1 + 16p + 156p^2 + 896p^3 + 2396p^4)C^4, \quad (\text{B6})$$

which, with increasing p , increases from the Gaussian value $\mu_4(0) = 3$, to the value $\mu_4(1) = 46.2$. Hence there is a one-to-one correspondence between p and $\mu_4(p)$.

(3) For $p=0$, $G^3(0)$ is the standardized Gaussian. For $p=1$, the PDF of $G^3(1)$ is

$$f_1(z) = \frac{15^{1/6} \exp\left(-\frac{1}{2}15^{1/3}|z|^{2/3}\right)}{3(2\pi)^{1/2}|z|^{2/3}}. \quad (\text{B7})$$

Note that $f_1(z)$ has an integrable singularity at $z=0$.

(4) For $0 < p < 1$, $f_p(z)$ is finite, monomodal, with tails (i.e., $|z| \rightarrow \infty$)

$$f_p(z) \sim \frac{\exp\left(-\frac{1}{2}(Cp)^{-2/3}|z|^{2/3}\right)}{3(2\pi)^{1/2}(Cp)^{1/3}|z|^{2/3}}. \quad (\text{B8})$$

- ¹P. K. Yeung, "One- and two-particle Lagrangian acceleration correlations in numerically simulated homogeneous turbulence," *Phys. Fluids* **9**, 2981 (1997).
- ²G. A. Voth, K. Satyanarayan, and E. Bodenschatz, "Lagrangian acceleration measurements at large Reynolds number," *Phys. Fluids* **10**, 2268 (1998).
- ³P. Vedula and P. K. Yeung, "Similarity scaling of pressure and acceleration statistics in numerical simulations of turbulence," *Phys. Fluids* **11**, 1208 (1999).
- ⁴A. LaPorta, G. A. Voth, A. M. Crawford, J. Alexander, and E. Bodenschatz, "Fluid particle accelerations in fully developed turbulence," *Nature (London)* **409**, 1017 (2001).
- ⁵G. A. Voth, A. LaPorta, A. M. Crawford, J. Alexander, and E. Bodenschatz, "Measurement of particle accelerations in fully developed turbulence," *J. Fluid Mech.* **469**, 121 (2002).
- ⁶R. J. Hill, "Scaling of acceleration in locally isotropic turbulence," *J. Fluid Mech.* **452**, 361 (2002).
- ⁷S. B. Pope, "A Stochastic Lagrangian model for acceleration in turbulent flows," *Phys. Fluids* **14**, 2360 (2002).
- ⁸K. Christensen and R. J. Adrian, "Measurement of instantaneous Eulerian acceleration fields by particle image accelerometry: Method and accuracy," *Exp. Fluids* **33**, 759 (2002).
- ⁹A. M. Reynolds, "On the application of nonextensive statistics to Lagrangian turbulence," *Phys. Fluids* **15**, L1 (2003).
- ¹⁰A. M. Reynolds, "Superstatistical mechanics of tracer particle motions in turbulence," *Phys. Rev. Lett.* **91**, 084503 (2003).
- ¹¹B. L. Sawford, P. K. Yeung, M. S. Borgas, P. Vedula, A. M. Crawford, L. LaPorta, and E. Bodenschatz, "Acceleration variance and conditional variance statistics in turbulence," *Phys. Fluids* **15**, 3478 (2003).
- ¹²A. Gylfason, S. Ayyalasomayajula, and Z. Warhaft, "Intermittency, pressure and acceleration statistics from hot-wire measurements in wind-tunnel turbulence," *J. Fluid Mech.* **501**, 213 (2004).
- ¹³L. Biferale, G. Boffetta, A. Celani, B. J. Devenish, A. Lanotte, and F. Toschi, "Multifractal statistics of Lagrangian velocity and acceleration in turbulence," *Phys. Rev. Lett.* **93**, 064502 (2004).
- ¹⁴B. L. Sawford, "Reynolds number effects in Lagrangian stochastic models of turbulent dispersion," *Phys. Fluids A* **3**, 1577 (1991).
- ¹⁵K. R. Sreenivasan, "On the scaling of the turbulent energy dissipation rate," *Phys. Fluids* **27**, 1048 (1984).
- ¹⁶P. K. Yeung and S. B. Pope, "Lagrangian statistics from direct numerical simulations of isotropic turbulence," *J. Fluid Mech.* **207**, 531 (1989).
- ¹⁷R. O. Fox, "The Lagrangian spectral relaxation model of the scalar dissipation in homogeneous turbulence," *Phys. Fluids* **9**, 2364 (1997).
- ¹⁸S. B. Pope and Y. L. Chen, "The velocity-dissipation probability density function model for turbulent flows," *Phys. Fluids A* **2**, 1437 (1990).
- ¹⁹M. S. Chong, J. Soria, A. E. Perry, J. Chacin, B. J. Cantwell, and Y. Na, "Turbulence structures of wall-bounded shear flows using DNS data," *J. Fluid Mech.* **357**, 225 (1998).
- ²⁰A. Ooi, J. Martin, J. Soria, and M. S. Chong, "A study of the evolution and characteristics of the invariants of the velocity-gradient tensor in isotropic turbulence," *J. Fluid Mech.* **381**, 141 (1999).
- ²¹S. Lee and C. Lee, "Intermittency of acceleration in isotropic turbulence," *Phys. Rev. E* **71**, 056310 (2005).
- ²²P. K. Yeung, D. A. Donzis, and K. R. Sreenivasan, "High Reynolds number simulation of turbulent mixing," *Phys. Fluids* **17**, 081703 (2005).
- ²³V. Yakhot and K. R. Sreenivasan, "Anomalous scaling of structure functions and dynamic constraints on turbulence simulations," *J. Stat. Phys.* **121**, 823 (2005).
- ²⁴V. Eswaran and S. B. Pope, "An examination of forcing in direct numerical simulations of turbulence," *Comput. Fluids* **16**, 257 (1988).
- ²⁵R. S. Rogallo, "Numerical experiments in homogeneous turbulence," NASA Tech. Memo. 81315 (1981).
- ²⁶P. K. Yeung, "Correlations and conditional statistics in differential diffusion: scalars with mean scalar gradients," *Phys. Fluids* **10**, 2621 (1998).
- ²⁷P. K. Yeung and S. B. Pope, "Differential diffusion of passive scalars in isotropic turbulence," *Phys. Fluids A* **5**, 2467 (1993).
- ²⁸K. R. Sreenivasan, "An update on the energy dissipation rate in isotropic turbulence," *Phys. Fluids* **10**, 528 (1998).
- ²⁹P. Burattini, P. Lavoie, and R. A. Antonia, "On the normalized energy dissipation rate," *Phys. Fluids* **17**, 098103 (2005).
- ³⁰R. M. Kerr, "Higher-order derivative correlations and the alignment of small-scale structures in isotropic numerical turbulence," *J. Fluid Mech.* **153**, 31 (1985).
- ³¹G. K. Batchelor, *The Theory of Homogeneous Turbulence* (Cambridge University Press, Cambridge, 1953).
- ³²K. R. Sreenivasan and R. A. Antonia, "The phenomenology of small-scale turbulence," *Annu. Rev. Fluid Mech.* **29**, 435 (1997).
- ³³A. N. Kolmogorov, "A refinement of previous hypotheses concerning the local structure of turbulence in a viscous incompressible fluid at high Reynolds number," *J. Fluid Mech.* **13**, 82 (1962).
- ³⁴K. R. Sreenivasan and P. Kailasnath, "An update on the intermittency exponent in turbulence," *Phys. Fluids A* **5**, 512 (1993).
- ³⁵A. M. Obukhov, "Some specific features of atmospheric turbulence," *J. Fluid Mech.* **13**, 77 (1962).
- ³⁶U. Frisch, *Turbulence: The Legacy of A. N. Kolmogorov* (Cambridge University Press, Cambridge, 1995).
- ³⁷A. S. Monin and A. M. Yaglom, *Statistical Fluid Mechanics* (MIT Press, Cambridge, 1975).
- ³⁸S. B. Pope, "Lagrangian PDF methods for turbulent flows," *Annu. Rev. Fluid Mech.* **26**, 23 (1994).
- ³⁹T. Gotoh and R. S. Rogallo, "Intermittency and scaling of pressure at small scales in forced isotropic turbulence," *J. Fluid Mech.* **396**, 257 (2000).
- ⁴⁰M. S. Borgas, "The multifractal Lagrangian nature of turbulence," *Philos. Trans. R. Soc. London, Ser. A* **342**, 379 (1993).
- ⁴¹S. B. Pope, *Turbulent Flows* (Cambridge University Press, Cambridge, U.K., 2000).
- ⁴²M. S. Borgas and P. K. Yeung, "Conditional fluid particle accelerations in turbulence," *Theor. Comput. Fluid Dyn.* **11**, 69 (1998).
- ⁴³A. M. Reynolds, N. Mordant, A. M. Crawford, and E. Bodenschatz, "On the distribution of Lagrangian accelerations in turbulent flows," *New J. Phys.* **7**, 58 (2005).
- ⁴⁴P. K. Yeung and S. B. Pope, "An algorithm for tracking fluid particles in numerical simulations of homogeneous turbulence," *J. Comput. Phys.* **79**, 373 (1988).
- ⁴⁵K. R. Sreenivasan and C. Meneveau, "Singularities of the equations of fluid motion," *Phys. Rev. A* **38**, 6287 (1988).